Developmental Cell
Article

Wnt5a Directs Polarized Calcium Gradients by Recruiting Cortical Endoplasmic Reticulum to the Cell Trailing Edge

Eric S. Witze,[1,7] Mary Katherine Connacher,[1] Stephane Houel,[1,2] Michael P. Schwartz,[2,3,8] Mary K. Morphew,[4,6] Leah Reid,[1] David B. Sacks,[4,6] Kristi S. Anseth,[2,3,5] and Natalie G. Ahn[1,2,5,*]
[1]Department of Chemistry and Biochemistry
[2]Howard Hughes Medical Institute
[3]Department of Chemical and Biological Engineering
[4]Department of Molecular, Cellular, and Developmental Biology
[5]BioFrontiers Institute
University of Colorado, Boulder, CO 80309, USA
[6]Department of Laboratory Medicine, National Institutes of Health, Bethesda, MD 20892, USA
[7]Present address: Department of Cancer Biology, University of Pennsylvania, Philadelphia, PA 19104, USA
[8]Present address: Department of Biomedical Engineering, University of Wisconsin, Madison, WI 53706, USA
*Correspondence: natalie.ahn@colorado.edu
http://dx.doi.org/10.1016/j.devcel.2013.08.019

SUMMARY

Wnt5a directs the assembly of the Wnt-receptor-actin-myosin-polarity (WRAMP) structure, which integrates cell-adhesion receptors with F-actin and myosin to form a microfilament array associated with multivesicular bodies (MVBs). The WRAMP structure is polarized to the cell posterior, where it directs tail-end membrane retraction, driving forward translocation of the cell body. Here we define constituents of the WRAMP proteome, including regulators of microfilament and microtubule dynamics, protein interactions, and enzymatic activity. IQGAP1, a scaffold for F-actin nucleation and crosslinking, is necessary for WRAMP structure formation, potentially bridging microfilaments and MVBs. Vesicle coat proteins, including coatomer-I subunits, localize to and are required for the WRAMP structure. Electron microscopy and live imaging demonstrate movement of the ER to the WRAMP structure and plasma membrane, followed by elevation of intracellular Ca^{2+}. Thus, Wnt5a controls directional movement by recruiting cortical ER to mobilize a rear-directed, localized Ca^{2+} signal, activating actomyosin contraction and adhesion disassembly for membrane retraction.

INTRODUCTION

Directional movement in migrating cells requires integrating processes that control motility and cell polarization, allowing cells to distinguish front from back. At the leading edge are events controlling F-actin assembly, mediated by the activation of Rac and Cdc42, Arp2/3 and formins, PIP kinases, and actin-severing proteins. These leading-edge components drive actin nucleation and polymerization, forming membrane protrusions and sheet extensions that in turn facilitate attachments between integrin receptors and extracellular matrix proteins (Parsons et al., 2010). Also important are processes controlling microtubule assembly and orientation as well as localized vesicle exocytosis to replenish cell-surface integrins, modulated through transient Ca^{2+} fluctuations at the front end of cells (Wei et al., 2009). Cell-polarity effectors, such as Scribble and PARtition protein complexes, direct trafficking of proteins to the front of migrating cells, enabling localized activation of Rac and Cdc42 (Petrie et al., 2009).

At the cell trailing edge are RhoA and Rho kinase-dependent processes leading to contractility driven by F-actin and myosin II, which reduce cell volume and create transient mechanical force to drive forward translocation (Cramer, 2010). Rear-end dynamics are driven by phosphorylation of myosin light chain via Ca^{2+}-calmodulin-dependent myosin light-chain kinase (MLCK) as well as recruitment of the Ca^{2+} protease calpain, which degrades focal adhesion proteins and allows focal adhesion disassembly (Petrie et al., 2009). Thus, directional movement involves coordination between localized membrane protrusions and formation of cell adhesions at the leading edge and membrane retraction and disassembly of adhesions at the rear. At the tail end of moving cells, free Ca^{2+} is needed to activate multiple enzymes, and in some polarized migrating cell types a gradient of Ca^{2+} elevated at the rear and decreasing to the front has been demonstrated (Hahn et al., 1992; Brundage et al., 1991). However, little is known about signaling mechanisms that recruit proteins and allow Ca^{2+} release, polarized to the rear.

We reported that Wnt5a promotes the assembly of the Wnt-receptor-actin-myosin-polarity (WRAMP) structure, which includes melanoma cell adhesion molecule (MCAM/CD146/MUC18) as well as Frizzled-3, F-actin, and myosin II (Witze et al., 2008). The WRAMP structure is associated with a dense microfilamentous array surrounding a vesicle pool consisting of multivesicular bodies (MVBs). Its formation requires dynamin and Rab4, revealing a role for vesicle trafficking in Wnt5a-regulated cell polarization. The WRAMP structure forms dynamically

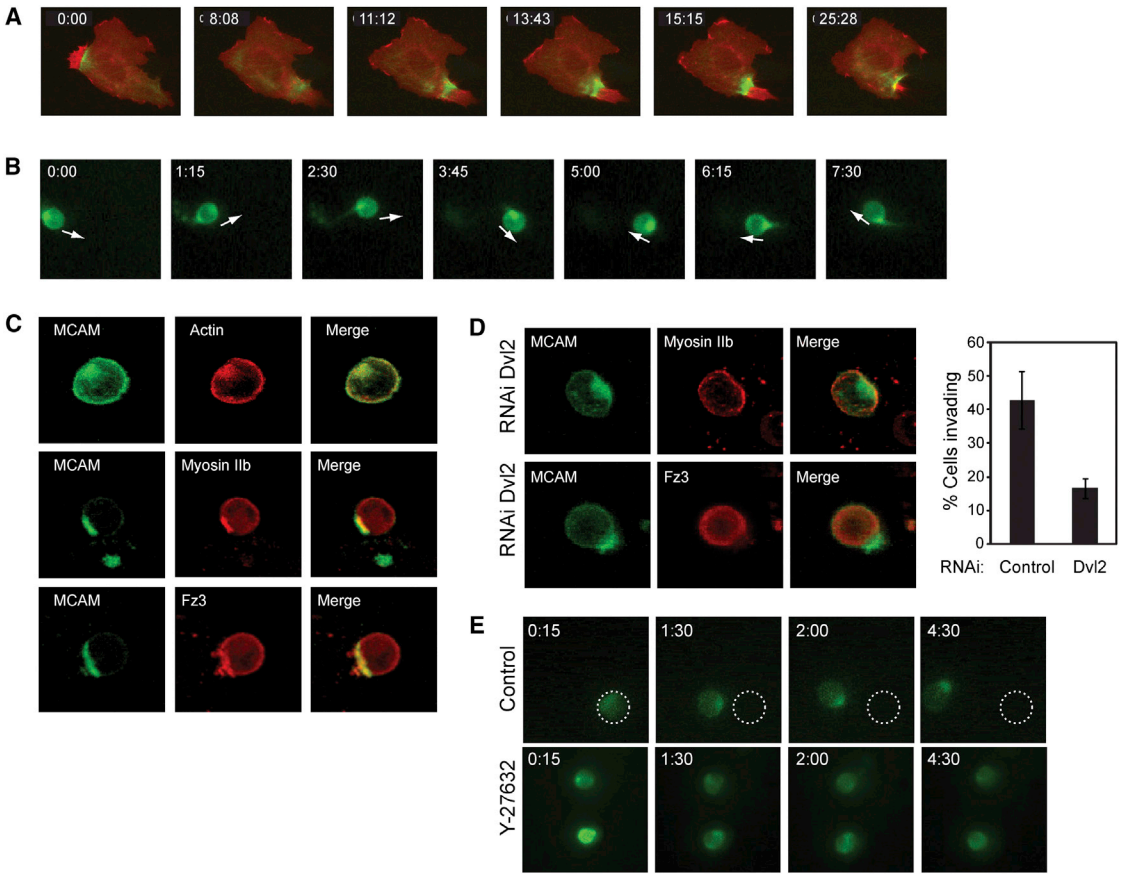

Figure 1. The WRAMP Structure Polarizes to the Cell Posterior during Invasion

(A) WM239A cells transfected with MCAM-RFP and GFP-myosin IIb heavy chain on 2D plates show the WRAMP structure, characterized by polarization of MCAM and myosin IIb, followed by membrane retraction (see Movie S1). Time indicates min:s. See also Figure S1.

(B) In cells transfected with MCAM-GFP invading in 3D hydrogels, MCAM stably localizes at the cell rear relative to the direction of movement, indicated by arrows (see Movie S1).

(C) Immunocytochemistry shows that endogenous myosin IIb, Frizzled-3, and F-actin localize with MCAM to the WRAMP structure in hydrogels.

(D) Dvl2 knockdown blocks myosin IIb and Frizzled-3 recruitment to the WRAMP structure in hydrogels. The bar graph quantifies percentages of cells that form WRAMP structures in this experiment (±SD, n = 200–400 cells).

(E) ROCK inhibitor Y27632 interferes with MCAM-GFP polarization and inhibits cell invasion (see Movie S1). The dotted circles represent the location of the cell at t = 0.

Time in (B)–(E) indicates hr:min.

and is directed toward the cell posterior, followed within minutes by tail-end membrane retraction, allowing nucleokinesis in the direction of cell movement (Figure 1A; Movie S1 available online). Thus, Wnt5a controls forward cell movement in part by polarized assembly of the WRAMP structure, which integrates receptors, cytoskeletal proteins, and MVBs through a mechanism involving receptor endocytosis and endosome trafficking, and directs membrane retraction at the trailing edge.

Little is known about the composition or function of the WRAMP structure or how it promotes membrane retraction. Here we present a proteomics strategy to define constituents of the WRAMP structure proteome by mass spectrometry, and report proteins involved in microfilament and microtubule dynamics as well as membrane organellar function. In particular, subunits of the COP-I coatomer predict a potential involvement of the Golgi/endoplasmic reticulum (ER). The WRAMP structure modulates rear-directed recruitment of cortical ER followed by the elevation of free Ca^{2+}, explaining how Ca^{2+} signaling can occur in a polarized manner in order to promote substrate detachment and actomyosin contractility, events needed for membrane retraction.

RESULTS

In response to Wnt5a, cells form the WRAMP structure, which assembles dynamically and coordinates the colocalization of MCAM, F-actin, and myosin IIb, followed by membrane retraction (Figure 1A; Figure S1A; Movie S1). Although the experiments in this study are performed in WM239A melanoma cells, we observe the WRAMP structure in other cell types, such as HUVEC and C2C12 (Figures S1B and S1C). In 2D cultured cells, WRAMP structures polarize distal to the Golgi, consistent with its rear-directed localization at the trailing edge (Witze et al., 2008).

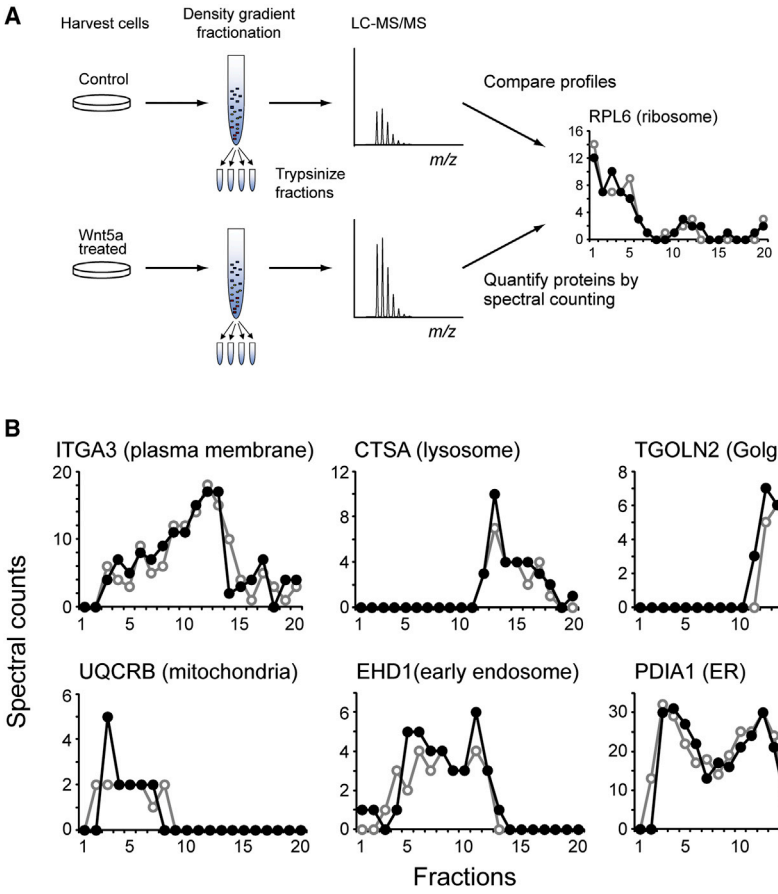

Figure 2. Proteomics Profiling of Organelle Fractions

(A) WM239A cells were lysed and postnuclear membranes were fractionated by density gradient centrifugation, followed by protein digestion and LC-MS/MS. Protein abundances were quantified by spectral counting.

(B) Spectral count profiles of protein organelle markers show few differences between cells treated with (●) or without (○) Wnt5a for 30 min. See also Table S1.

Because little is known about the WRAMP structure in 3D environments, we examined cells using an engineered extracellular matrix in order to limit other signaling influences (Fairbanks et al., 2009). WM239A cells expressing MCAM-GFP were encapsulated in photopolymerizable hydrogels crosslinked to matrix metalloproteinase (MMP)-degradable peptides and pendant peptides containing the Arg-Gly-Asp (RGD) integrin recognition motif. The resulting 3D hydrogel promotes cell spreading and migration through protease- and adhesion-dependent processes.

Live imaging showed cells invading through the 3D matrix with clear evidence for stable rear polarization of MCAM-GFP (Figure 1B; Movie S1). Immunocytochemistry revealed colocalization of MCAM with F-actin, myosin IIb, and the Wnt5a receptor Frizzled-3 (Figure 1C). Recruitment of myosin IIb and Frizzled-3 to the WRAMP structure was inhibited when Wnt signaling was disrupted by RNAi knockdown of Dishevelled (Figure 1D). Polarization of MCAM was also disrupted when cells were treated with the Rho kinase inhibitor Y27632 (Figure 1E; Movie S1), or when RGD ligand was replaced with a scrambled peptide to prevent integrin binding (data not shown). These results demonstrated that the WRAMP structure formed in 3D is analogous to that previously observed in 2D, with polarization being dependent on Wnt signaling via Dishevelled, cell-matrix interactions, and Rho kinase-dependent mechanisms. Surprisingly, the WRAMP structure forms stably at the rear of WM239A cells for many hours in 3D, in contrast to 2D culture, where it forms transiently. This provides an important illustration of how local environment profoundly influences the polarity of invasive cancer cells.

We next looked for other components within the WRAMP structure. Cells were harvested after 30 min of Wnt5a treatment, and postnuclear membrane preparations were separated by density gradient centrifugation. Proteins in each fraction were trypsinized, and peptides were identified by LC-MS/MS (Figure 2A). Label-free quantification by spectral counting (Old et al., 2005) was used to identify proteins altered in abundance or elution in response to Wnt5a. In total, 3,015 proteins were identified (Table S1), which included protein markers for all major organelle classes, including ER, Golgi, mitochondria, plasma membrane microsomes, early and late endosomes, lysosomes, and peroxisomes (Figure 2B). Most proteins were unaffected by Wnt5a, but in 36 proteins the spectral counts increased by 2-fold or more within a single fraction at high density (fraction 2, Figures 3A–3G; Figure S2). Myosin IIb was also present in the data set, although with low spectral counts (Figure 3H). The results suggested that Wnt5a elevates the abundance of certain proteins within a specific organelle pool.

We asked whether the proteins within this pool were associated with the WRAMP structure, by monitoring their colocalization with MCAM by indirect immunocytochemistry (Figure 3). Endogenous forms of every protein tested localized with or in proximity to the WRAMP structure. The results showed that proteins within the WRAMP structure were stable to density gradient purification and could be identified by their increased abundance within a high-density fraction in response to Wnt5a. We conclude that proteins identified in this manner represent initial components of the WRAMP proteome.

Constituents of the WRAMP proteome included known regulators of microfilament and microtubule dynamics, cell adhesion and movement, and membrane trafficking, as well as proteins with enzymatic and protein recognition functions (Table S2). Examples included IQGAP1 and filamin-A, microfilament-binding proteins that crosslink actin filaments, and gelsolin, an actin-severing protein that promotes microfilament turnover and

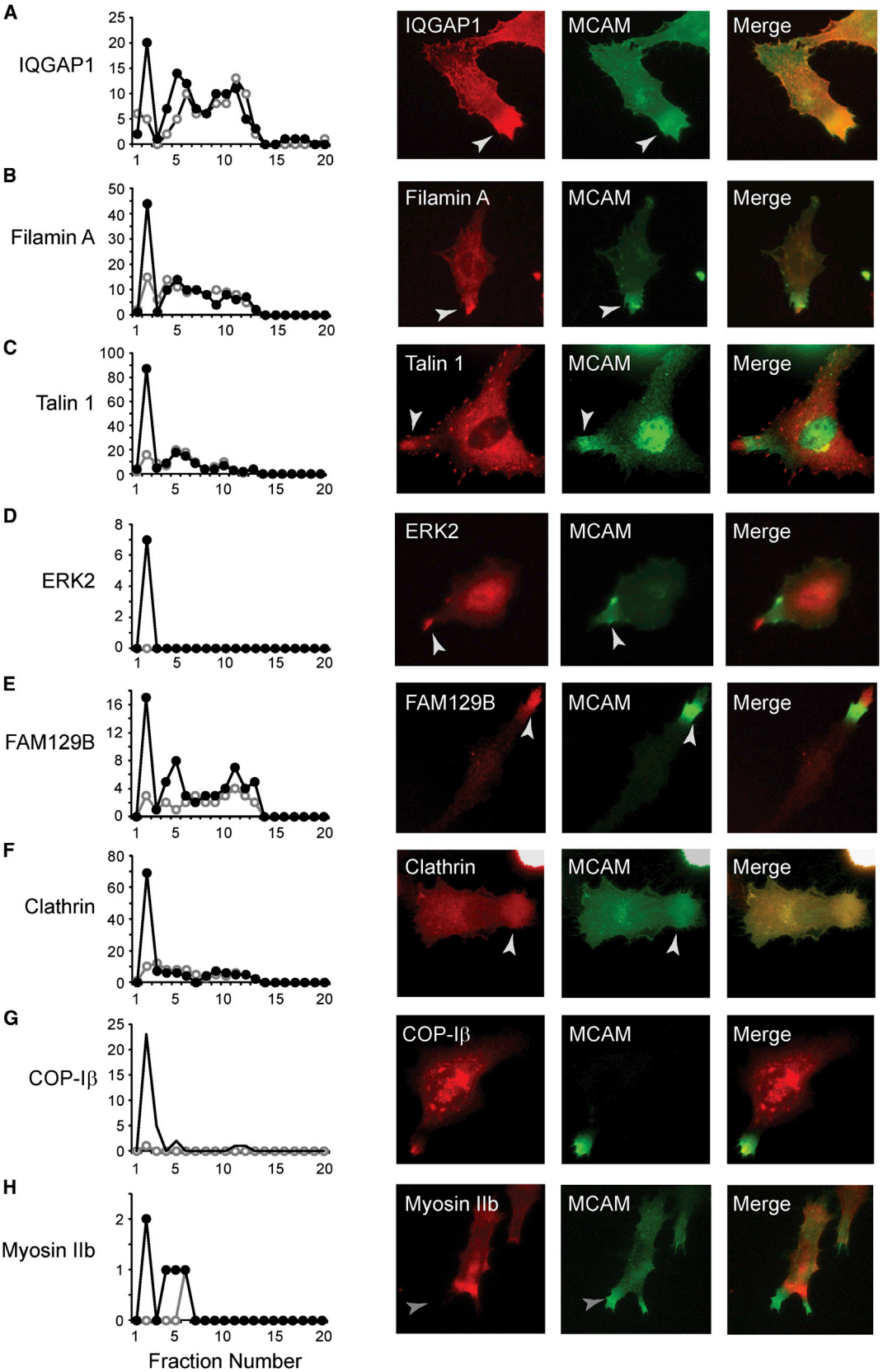

(legend on next page)

branching (Nakamura et al., 2011; Yin and Stossel, 1979). Also present was the microfilament motor myosin IIa, whose structure and function is related to myosin IIb. Myosin 1b, containing binding domains for calmodulin and phosphatidylinositol phospholipids, is a class I myosin motor that bridges actin-membrane interactions and also associates with and facilitates trafficking of proteins into MVBs (Salas-Cortes et al., 2005). Other components included focal adhesion proteins talin-1 and kindlin-3/UNC112, both of which mediate protein interactions needed for integrin receptor activation, enabling linkages between F-actin and the extracellular matrix (Burridge and Connell, 1983; Moser et al., 2008). Microtubule regulators included tubulin-α1b and dynein, as well as nuclear migration protein nudC, a chaperone that mediates interactions between kinesin, dynein, and dynactin (Yamada et al., 2010). Noncytoskeletal proteins included calpain-2 and the ERK2 MAP kinase, which have been shown to promote focal adhesion disassembly via ERK phosphorylation of calpain and proteolysis of focal adhesion proteins (Glading et al., 2001). FAM129B/Minerva was previously identified as a target of ERK phosphorylation, which mediates oncogenic B-Raf-dependent melanoma cell invasion (Old et al., 2009). Finally, the WRAMP proteome contained regulators of vesicle internalization and trafficking, including the vesicle coat proteins, clathrin, and the α, β, γ, and δ subunits of the coatomer protein I complex (COP-I).

Experiments were performed to test the functional importance of constituent proteins in WRAMP structure formation. IQGAP1 is an adaptor protein that forms a scaffold for actin nucleation by N-WASP/Arp2/3 (Le Clainche et al., 2007). Immunocytochemistry showed that after treatment with Wnt5a, endogenous IQGAP1 localized to the WRAMP structure marked by MCAM-GFP in 2D and 3D cell environments (Figure 4A). RNAi depletion of IQGAP1 interfered with WRAMP structure assembly, blocking polarization of MCAM, myosin IIb, and F-actin (Figures 4B and 4C). Furthermore, immunoprecipitation of MCAM revealed its interactions with endogenous IQGAP1 (Figure 4D). Thus, IQGAP1 is functionally important for WRAMP structure assembly and binds MCAM. Immunoprecipitation of the endogenous Wnt adaptor protein Dishevelled also revealed MCAM binding (Figure 4E). Thus, our working model is that MCAM is directly linked to Wnt5a/Dvl/Fz signaling, and that assembly of the WRAMP structure is driven in part by adaptor proteins such as IQGAP1, which bridge interactions between MCAM and cytoskeletal proteins.

The presence of COP-I subunits within the WRAMP proteome was unexpected, because these proteins have to our knowledge never been linked to cell polarity. Instead, COP-I facilitates retrograde vesicle transport from the Golgi to the ER within ER-Golgi intermediate compartment (ERGIC) organelles, by binding cargo proteins containing C-terminal dilysine motifs (e.g., $KKXX_{C\text{-term}}$, $KXKXX_{C\text{-term}}$), which are canonical signals for ER retrieval. Nevertheless, in response to Wnt5a, COP-I α, β, γ, and δ subunits were elevated within the high-density fraction (Figure 3; Figure S2). Immunocytochemistry of endogenous COP-Iβ revealed its juxtanuclear localization, consistent with primary recruitment to ERGIC. However, a subfraction of COP-Iβ colocalized with the WRAMP structure at the membrane periphery, in cells cultured on plates or in hydrogels (Figures 3G and 5A). Coimmunoprecipitation experiments showed that COP-Iβ binds MCAM in a Wnt5a-dependent manner (Figure 5B). RNAi knockdown of COP-Iβ inhibited formation of the WRAMP structure in response to Wnt5a (Figures 5C and 5D). Following COP-Iβ depletion, the levels of MCAM remained constant; however, its localization changed to a perinuclear pattern overlapping with markers for the Golgi (58 kDa protein) and early endosomes (EEA1) (Figure 5E). Together, the results suggested a potential role for the Golgi or ER in the formation and/or function of the WRAMP structure.

These findings prompted closer examination of the WRAMP ultrastructure. MCAM-GFP-expressing cells were treated with Wnt5a for 30 min and then monitored for the appearance and placement of WRAMP structures. Cells were then fixed and stained and analyzed by correlative electron microscopy (EM) and tomographic reconstruction of 250 nm sections. Figure 6A shows the 3D reconstruction of a WRAMP structure region. Here, dense filamentous structures consistent with F-actin (yellow) formed extended cables aligned in parallel. MVBs (blue) were identifiable by the presence of intralumenal vesicles of 100- to 120-nm diameter (green). MCAM-GFP was also monitored after Wnt5a treatment by transmission immuno-EM using anti-GFP-coupled gold particles. MCAM was clearly observed in the plasma membrane as well as the limiting membranes and intralumenal vesicles of MVBs appearing within the WRAMP structure (Figure 6B).

Strikingly, the WRAMP structure was filled with a network of contiguous membrane sheets and tubules (Figure 6A). These were in some places juxtaposed closely to the plasma membrane (Figure 6C), suggesting a network of cortical ER. At the cell periphery, the ER localized to the end of the WRAMP structure, and bundles of actin extended from the edge of the cell to form larger actin cables. This appearance contrasted with that outside the WRAMP structure, where the ER appeared more sheet like within regions intermediate between the nucleus and trailing edge. Here, endosomal vesicles were present whereas MVBs were mostly absent, and F-actin appeared less dense with short crossed filament bundles.

Ultrastructural studies revealed that the WRAMP structure is associated with an ER pool in close proximity to the plasma membrane, which forms a network with actin filaments. In order to examine the relationship between the ER and the WRAMP structure, cells were cotransfected with MCAM-GFP and a protein fusion between the KDEL (Lys-Asp-Glu-Leu) ER protein retention motif and monomeric red fluorescent protein (ER-RFP). Live imaging showed that ER-RFP was recruited dynamically to the WRAMP structure and the membrane edge prior to membrane retraction (Figure 6D; Movie S2). We also found that calnexin, an integral membrane protein in the ER that functions in protein folding, colocalized with MCAM in the WRAMP

Figure 3. Components of the WRAMP Proteome

Spectral counts of identified proteins versus fraction number (highest density in fraction 1) in cells treated with (●) or without (○) Wnt5a. Several proteins showed increased abundance in fraction 2 in response to Wnt5a. In each case, immunocytochemistry showed colocalization with endogenous MCAM, indicating recruitment to the WRAMP structure. See also Figure S2 and Table S2. The arrowheads indicate the location of the WRAMP structure.

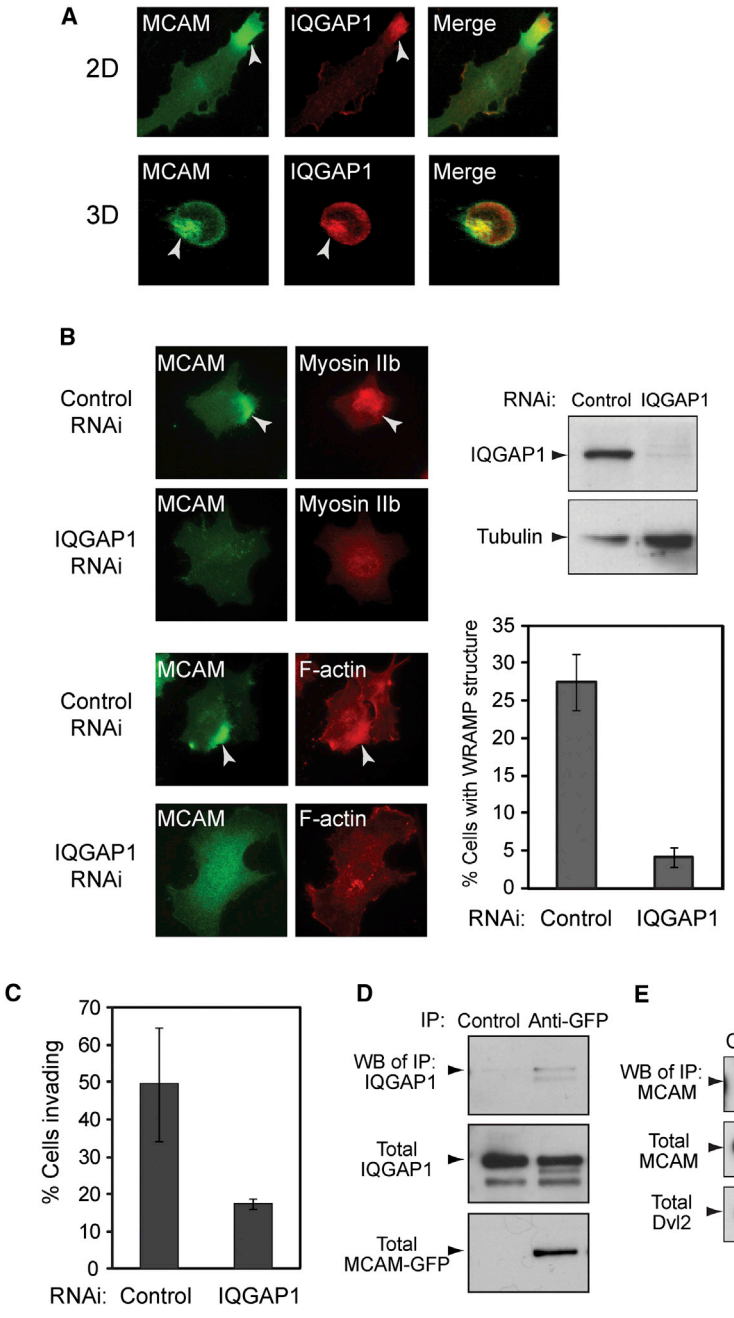

Figure 4. IQGAP1 Colocalizes with the WRAMP Structure and Is Required for Its Formation

(A) MCAM-GFP and endogenous IQGAP1 were monitored by immunocytochemistry in cells on plates (top) or within hydrogels (bottom). IQGAP1 colocalizes with MCAM at the WRAMP structure in both 2D and 3D culture. The arrowheads indicate the location of the WRAMP structure.

(B) Cells in 2D were treated with nontargeting or IQGAP1-RNAi oligonucleotides prior to Wnt5a. Monitoring MCAM-GFP, endogenous myosin IIb, and F-actin shows that knockdown of IQGAP1 inhibits formation of the WRAMP structure. Cells were quantified for the WRAMP structure, monitored with MCAM-GFP (±SD, n = 3, each counting 200–350 cells).

(C) Cells in hydrogels were quantified for invasion, which was inhibited by RNAi knockdown of IQGAP1. Invasion was scored by the movement of a cell within the hydrogel by one cell length or more (±SD, n = 3, each counting 330–380 cells).

(D) Immunoprecipitation of MCAM-GFP revealed binding to endogenous IQGAP1.

(E) Immunoprecipitation of endogenous Dvl2 revealed association with MCAM-GFP in cells treated for 30 min with Wnt5a.

structure (Figure 6E). Treatment of cells with Brefeldin A, which blocks recruitment of COP-I to membrane vesicles, also blocked WRAMP structure formation (Figure 6F). Whereas ER-RFP and calnexin always colocalized with the WRAMP structure in Wnt5a-treated cells, the association of these ER markers was inhibited in cells treated with Brefeldin A or RNAi-COP-Iβ (data not shown). Thus, the WRAMP structure is associated with polarized movement of the ER to the plasma membrane in a manner that depends on COP-I. Recruitment of this ER pool is coordinated with WRAMP structure assembly, where it moves past MCAM to the membrane periphery and precedes membrane retraction at the trailing edge.

The movement of ER to the WRAMP structure led us to hypothesize its involvement in polarized Ca^{2+} mobilization. Wnt5a is known to signal via Ca^{2+} and calmodulin, and Ca^{2+} release coupled to cortical ER has been implicated during the recruitment of proteins to focal adhesions in response to proinflammatory cytokines (Wang et al., 2006). In addition, the ER is juxtaposed against the plasma membrane in response to Ca^{2+} depletion, enabling interactions between the ER Ca^{2+} sensor STIM1 and plasma membrane CRAC-M Ca^{2+} ion channels (Wu et al., 2006; Park et al., 2009; Orci et al., 2009). Recruitment of cortical ER has been shown to involve Ist2p, an ER protein with a C-terminal dilysine motif that binds COP-I in vitro (Lavieu et al., 2010; Ercan et al., 2009). Thus, movement of the ER to the cell periphery might involve COP-I interactions with proteins found within an ER subdomain.

Although our cells were not Ca^{2+} depleted, the precedent that cortical ER, recruited through COP-I, mediates Ca^{2+} influx prompted us to hypothesize that the WRAMP structure might similarly function to mobilize Ca^{2+} at the cell posterior. At the trailing edge, Ca^{2+} would be needed to promote membrane detachment and retraction catalyzed by Ca^{2+}-dependent proteases and MLCK. This possibility was supported by the appearance of calpain-2 and myosin II within the WRAMP proteome (Figure 7A; Figures S2C and S2M). Immunocytochemistry showed that both calpain-2 and phosphorylated myosin light

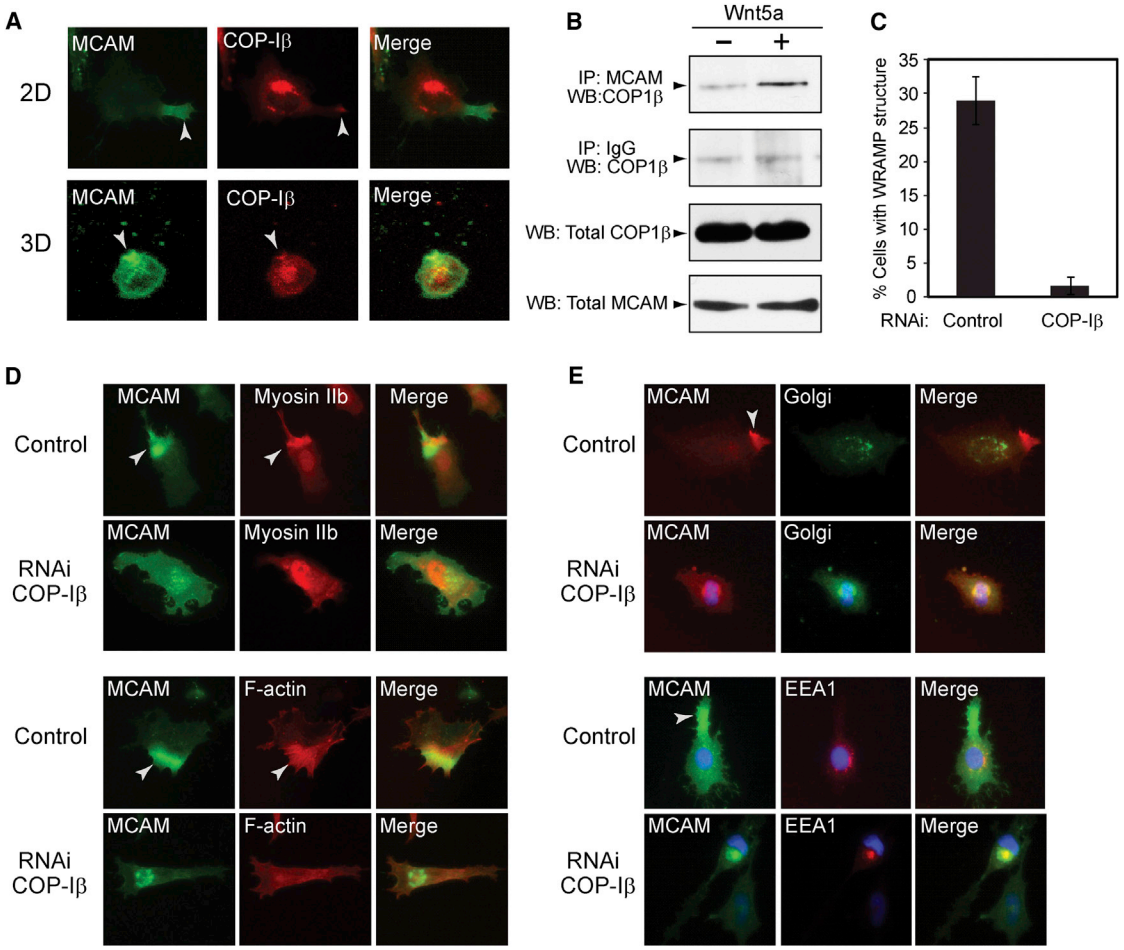

Figure 5. COP-Iβ Colocalizes with the WRAMP Structure and Is Required for Its Formation

(A) MCAM-GFP and endogenous COP-Iβ were monitored by immunocytochemistry in cells on plates (top) or within hydrogels (bottom). COP-Iβ colocalizes with MCAM at the WRAMP structure in 2D and 3D culture. The arrowheads indicate the location of the WRAMP structure.

(B) Endogenous MCAM was immunoprecipitated with αMCAM antibody, and western blots of pull-downs were probed for MCAM and COP-Iβ.

(C) Cells on plates were quantified for the WRAMP structure, monitored by endogenous MCAM polarization (±SD, n = 3, each counting 200–350 cells).

(D) Monitoring MCAM-GFP, endogenous myosin IIb, and F-actin shows that RNAi knockdown of COP-Iβ inhibits the WRAMP structure.

(E) After COP-Iβ knockdown, endogenous MCAM appears perinuclear, overlapping the 58 kDa Golgi protein marker and the early endosome marker EEA1.

chain colocalized with MCAM, suggesting that Ca^{2+}-dependent enzymes are recruited to the WRAMP structure and may participate in membrane retraction.

We tested this hypothesis by transfecting cells with the Cameleon FRET biosensor and ER-RFP to simultaneously monitor free Ca^{2+} and ER dynamics. Live-cell imaging showed increased Cameleon-FRET signal following the recruitment of ER-RFP to the WRAMP structure and preceding membrane retraction (Figure 7B; Movie S3). Similar responses were observed in cells coexpressing Cameleon and IQGAP1-RFP (data not shown). The results show that cytosolic Ca^{2+} increases transiently at the cell trailing edge, concomitant with WRAMP structure assembly and ER recruitment. Within the WRAMP structure, free Ca^{2+} transiently spiked to 0.8 μM from its basal concentration of 0.1 μM, whereas outside the WRAMP structure, Ca^{2+} remained unchanged (Figure S3).

The importance of localized cytosolic Ca^{2+} for membrane retraction was examined using inhibitors that block Ca^{2+} mobilization. SKF-96365, 2-aminoethoxydiphenylborane (2-APB), and ryanodine, respectively, inhibit Ca^{2+} influx through plasma membrane voltage-gated Ca^{2+} channels and ER-associated IP_3 and ryanodine receptors. Cells were pretreated with a combination of SKF-96365+ryanodine for 1 hr and then treated with Wnt5a and monitored live for MCAM-GFP. In response to SKF-96365-+ryanodine, membrane retraction was consistently repressed and replaced by membrane ruffles extending from the WRAMP structure (Figure 7C; Movie S3). Such effects were not observed when the inhibitors were applied separately (not shown), implying that Ca^{2+} mobilization depends on activation of ion channels within both the ER and plasma membrane. Likewise, 2-APB, an antagonist of IP_3 receptors and store-operated Ca^{2+} entry Trp channels, led to WRAMP structure disassembly and repressed membrane retraction when drug was added at 7 min at the moment of WRAMP structure formation (Figure 7C; Movie S3). Both events were derepressed when the inhibitor was subsequently removed at 24 min (Movie S3). Together, these results

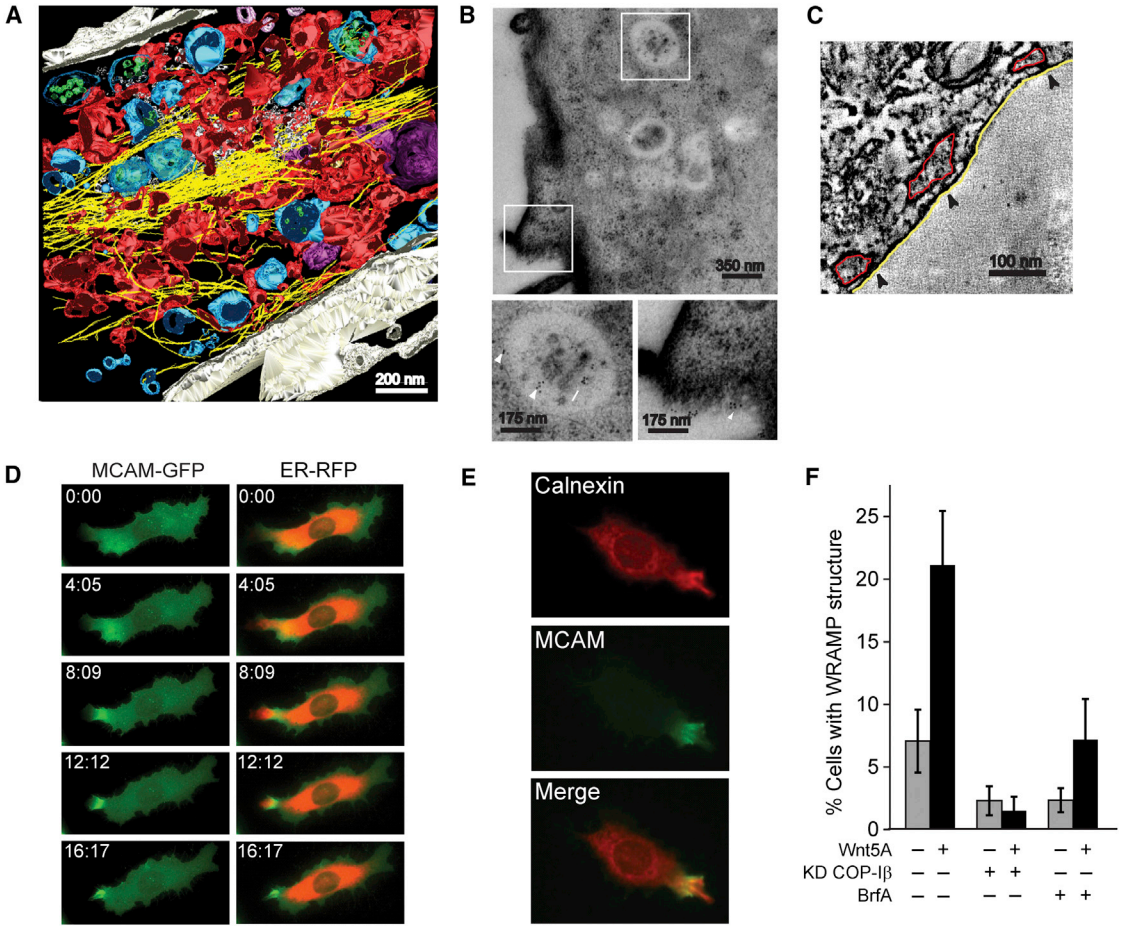

Figure 6. Cortical ER Is Recruited to the WRAMP Structure

(A) EM tomography showing the WRAMP structure in a cell treated with Wnt5a. Colors indicate MVBs (blue) and microfilaments (yellow) interspersed among ER tubules and sheets (red) that extend toward the edge of the cell.

(B) Immuno-EM using anti-GFP antibodies labeled with gold particles reveals the presence of MCAM-GFP (arrowheads) within intralumenal vesicles and limiting membranes of MVBs and at the plasma membrane. Bottom panels show magnified boxes in white.

(C) EM tomographs indicate cortical ER (red) juxtaposed within 10 nm of the plasma membrane (white).

(D) Live imaging of cells expressing MCAM-GFP and ER-RFP reveals localization of ER-RFP to the WRAMP structure, preceding membrane retraction (see Movie S2).

(E) Indirect immunofluorescence reveals localization of endogenous calnexin to the WRAMP structure.

(F) Pretreatment of cells with Brefeldin A or RNAi knockdown of COP-Iβ blocks WRAMP structure formation. Cells on plates were quantified for the WRAMP structure, monitored by endogenous MCAM polarization (±SD, n = 3, each counting 200–350 cells).

demonstrate a role for the WRAMP structure in directing membrane retraction events by elevating free Ca^{2+} at the trailing edge.

We also tested the importance of calpain, which was recruited to the WRAMP structure and trailing-edge membrane (Figure 7A). The cell-permeable calpain inhibitor MDL-28170 (calpain inhibitor III) did not affect the integrity of the WRAMP structure, but blocked membrane retraction and in fact led to membrane protrusions outward from the WRAMP structure (Figure 7C; Movie S3). Calpain inhibitor III decreased the number of cells exhibiting membrane retraction from 95% ± 5% (n = 13) to 36% ± 10% (n = 24) after forming a WRAMP structure. Thus, Ca^{2+} polarization by the WRAMP structure appears important for modulating proteolytic events involved in membrane detachment and retraction.

DISCUSSION

Our study demonstrates that rear-end cell polarization by Wnt5a involves active recruitment of cortical ER in coordination with the WRAMP structure. This finding was prompted by analyses of the WRAMP structure proteome, which revealed the presence of COP-I, suggesting an involvement of the ER in WRAMP structure formation. The temporal coordination between the movement of ER-RFP and calnexin ER markers to the WRAMP structure, enhanced Cameleon signal, and membrane retraction suggests that the order of events triggered by WRAMP structure assembly involves ER recruitment followed by elevation of free Ca^{2+} at the cell posterior. This would in turn activate localized Ca^{2+}-dependent enzymes, releasing matrix attachments and allowing membrane retraction. The model is supported by the disruption of

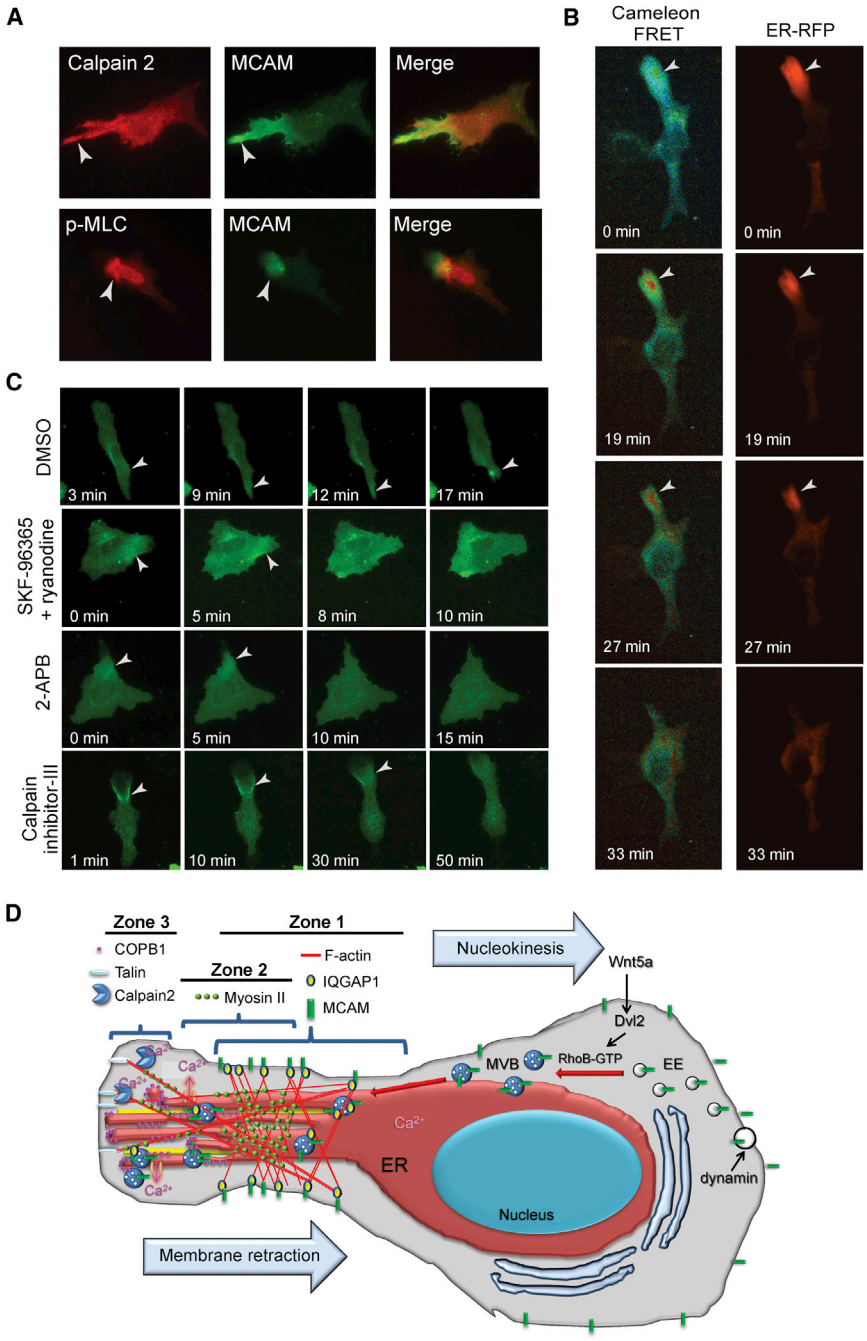

Figure 7. Coordination between the WRAMP Structure and Ca^{2+} Release

(A) Immunocytochemistry of Wnt5a-treated cells shows recruitment of calpain-2 and phosphorylated myosin light chain to MCAM-GFP in the WRAMP structure. The arrowheads indicate the location of the WRAMP structure.

(B) Cells expressing Cameleon and ER-RFP show elevation of free Ca^{2+} accompanying ER recruitment, followed by membrane retraction (see Movie S3). See also Figure S3.

(C) In cells expressing MCAM-GFP, Ca^{2+} channel inhibitors interfere with WRAMP-associated membrane retraction. DMSO control shows normal membrane retraction following WRAMP structure formation. Retraction is blocked by treatment with SKF-96365+ryanodine prior to Wnt5a (see Movie S3). 2-APB causes MCAM-GFP disassembly when added at 7 min at the moment of WRAMP structure formation (see Movie S3). Pretreating cells with calpain inhibitor III prior to Wnt5a blocks membrane retraction, causing membranes to instead protrude from the WRAMP structure (see Movie S3).

(D) A working model for the composition and function of the WRAMP structure, summarizing results from this and previous studies. In response to cell stimulation, MCAM and other receptors are internalized through dynamin-dependent endocytosis. The localization of MCAM within the MVBs and intralumenal vesicles associated with the WRAMP structure suggests that the assembly of the WRAMP structure occurs in part through trafficking of late endosomes that bypass the canonical pathway for lysosome degradation. This may involve RhoB, which is activated by Wnt5a and might inhibit lysosomal fusion. The appearance of tubulin, dynein, and nudC in the WRAMP proteome suggests an involvement of microtubules in polarized vesicle recruitment. The WRAMP structure consists of at least three overlapping subregions, or zones. MCAM, F-actin, and IQGAP1 begin assembling in zone 1, located farthest from the trailing edge. Live-cell imaging shows that these proteins dynamically translocate to the periphery, moving through zone 2 and finally arriving at zone 3, at the very tip of the trailing edge. We speculate that distinct events may occur within each subregion. For example, zone 1 might organize structures that initiate MVB recruitment and microfilament assembly. Zone 2 might serve to link MVBs to actomyosin, which is in turn linked to focal adhesion proteins in zone 3, which attach to transmembrane proteins and must be disassembled to allow membrane release. In this way, events that are spatially separated may combine to control the dynamics of the WRAMP structure and link organelle trafficking to membrane contractility.

WRAMP structure assembly by Brefeldin A and COP-Iβ knockdown, and by disruption of WRAMP-associated membrane retraction by inhibitors of ER- and plasma membrane-associated Ca^{2+} channels. Likely targets include calpain-2, which catalyzes disassembly of integrin-substrate attachments by proteolyzing focal adhesion proteins, and MLCK, which catalyzes myosin light-chain phosphorylation and actomyosin contraction. The coupling of these events to the WRAMP structure provides a mechanism that explains how the Wnt5a cell-polarity pathway directs intracellular Ca^{2+} gradients and directional movement via the polarized assembly of receptor-cytoskeletal complexes.

Combining these findings with previous results, we propose a working model for Wnt5a-mediated cell polarity, summarized in Figure 7D. In response to cell stimulation, MCAM and other receptors are internalized through dynamin-mediated endocytosis (Witze et al., 2008). The appearance of MCAM within MVBs and intralumenal vesicles associated with the WRAMP structure

suggests that the polarization of MCAM and the WRAMP structure occurs through trafficking of a late endosomal pool that bypasses the canonical pathway for lysosome-mediated degradation. This may involve RhoB, which we found to be activated by Wnt5a and might serve to prevent lysosomal fusion (Witze et al., 2008; Gampel et al., 1999). The appearance of tubulin and dynein in the WRAMP proteome, as well as nuclear migration protein nudC, which mediates interactions between kinesin, dynein, and dynactin (Yamada et al., 2010), suggests the involvement of microtubules in polarized vesicle recruitment and microtubule motors for vesicle targeting to the WRAMP structure. This is consistent with observations that nocodazole interferes with WRAMP structure formation (E.S.W. and N.G.A., unpublished data).

The WRAMP-associated MVBs might in turn recruit actomyosin through adaptor proteins that bind MCAM. For example, RhoB binds early and late endosomes and assembles actin cages around these vesicles by recruiting mDia1/2 formins (Wallar et al., 2007; Fernandez-Borja et al., 2005). IQGAP1, which is associated with and required for WRAMP structure formation, sustains nucleation of actin following formin activation by RhoA (Brandt et al., 2007), and could conceivably mediate vesicle-microfilament interactions by bridging MCAM and F-actin. MCAM binding to COP-I might in turn recruit the ER to the WRAMP structure, through interactions between COP-I and dilysine motif-containing proteins such as KDELR.

Recruitment of the ER may serve to localize Ca^{2+} release where it is needed at the site of membrane retraction. It was intriguing that ERK2 is present at the WRAMP structure in its active, phosphorylated form, along with the Ca^{2+}-dependent protease calpain-2 (Figures 3D and 7A). Localization of phospho-ERK at focal adhesions promotes calpain recruitment and protease activation, leading to proteolysis of focal adhesion proteins as a required step in adhesion disassembly (Carragher and Frame, 2004). ERKs also phosphorylate WRAMP proteins, including FAM129B/Minerva, which promotes melanoma cell invasion (Old et al., 2009).

Other proteins suggest the importance of microfilament and membrane protein interactions in the WRAMP structure. Filamin-A and gelsolin are actin-crosslinking and -severing proteins that could stabilize the dense F-actin bundles found within the WRAMP structure (Nakamura et al., 2011; Yin and Stossel, 1979). Talin-1 in the WRAMP structure might provide a means to anchor microfilaments to focal adhesions at the cortical plasma membrane. Kindlin3/FERMT3 binds talin-1 and the integrin β receptor, and modulates integrin activation and cell adhesion (Burridge and Connell, 1983; Moser et al., 2008). Filamin-A has a scaffold function, anchoring microfilaments to cell-adhesion receptors ICAM1, CEACAM1, and integrin β, and mediating the activation of signaling effectors such as Rho, ROCK, the RhoGEF Trio, and the RhoGAP FilGAP (Nakamura et al., 2011). Calpain cleaves interdomain linker regions in filamin-A, separating domains linking actin binding, homodimerization, and interactions with other binding partners. In melanoma cells, Wnt5a enhanced filamin-A proteolysis by calpain (O'Connell et al., 2009). This would provide a means by which localized Ca^{2+} release might disassemble the WRAMP structure, by disrupting MCAM-actin-plasma membrane interactions.

The localization of various components identified in this study suggests that the WRAMP structure is not a single homogeneous entity but contains at least three overlapping subregions, or zones (Figure 7D). MCAM, actomyosin, and IQGAP1 begin assembling in zone 1, located farthest from the trailing edge (Witze et al., 2008; Figures 1A and 3A). Live imaging shows that these proteins dynamically translocate to the periphery, moving through zone 2 and finally arriving at zone 3, the tip of the trailing edge. Our previous studies have shown that actin accumulation in zone 1 temporally follows MCAM (Witze et al., 2008). Clathrin also overlaps MCAM in zone 1, suggesting its potential association with MVBs. Zone 2 contains myosin IIb, partially overlapping MCAM but typically removed from zone 3 and the membrane edge prior to membrane retraction (Figures 1A and 3H; Movie S1). Zone 3 contains talin-1, filamin-A, calpain-2, and ERK2, which function in microfilament-membrane attachments and focal adhesion formation/turnover. We speculate that distinct events may occur within each subregion. For example, zone 1 might organize structures that initiate MVB recruitment and microfilament assembly. Zone 2 might link MVBs to actomyosin, which in turn links to focal adhesion proteins in zone 3 that attach to transmembrane proteins and must be disassembled to allow membrane release. In this way, events that are spatially separated may combine to control the dynamics of the WRAMP structure and link organelle trafficking to membrane contractility.

Our findings integrate different lines of evidence explaining how mechanisms controlling cell polarity allow cell movement, suggesting that analogous processes may occur in other systems. Indeed, polarized MCAM-GFP associates with tail-end retraction in HUVEC and C2C12 myoblast cells (Figure S1) and in HT1080 fibrosarcoma and adult hippocampal progenitor cells (data not shown). Polarized actomyosin structures also occur during neuronal migration and axonal pathfinding in cortical neurons, which mediate tail-end contraction and nucleokinesis, and are correlated with spatial Ca^{2+} transients (Martini and Valdeolmillos, 2010). In leukocytes and *Dictyostelium*, rear protrusions called uropods modulate trailing-edge movement by recruiting ezrin-radixin-moesin (ERM) proteins that assemble F-actin, myosin, and transmembrane receptors to the cell posterior (Sánchez-Madrid and Serrador, 2009). Uropods colocalize talin and F-actin, and myosin II-dependent force generation reorients microtubules to the cell posterior, where retraction is Ca^{2+} dependent (Eddy et al., 2002). In migrating lymphocytes, Ca^{2+} promotes release of uropods from the substrate through lysosomal fusion, which is mediated by synaptotagmin vesicle fusion proteins (Colvin et al., 2010). Finally, in *Dictyostelium*, adenylate cyclase is released at uropods during chemotaxis through a mechanism involving vesicle trafficking, secretion of MVBs, and exosome shedding (Kriebel et al., 2008). Such observations share similarities with the presence of actomyosin, MVBs, and Ca^{2+} in the WRAMP structure and its role in directing tail-end retraction during migration. Taken together, it seems likely that the WRAMP structure and its control of tail-end polarity are not restricted to melanoma cells but represents a general mechanism for controlling cell movement. Previous studies showed that Wnt5a, Fz, and Dvl modulate Ca^{2+} release (Kohn and Moon, 2005). This and the noted role of Wnt5a in polarized cell movement might explain why Wnt5a, of all Wnt ligands, can direct the assembly of the WRAMP structure.

A significant finding in our study is the evidence that rear-directed polarization involves dynamic movement of internal membrane pools, including MVBs, which recruit MCAM, and cortical ER, which promotes localized Ca^{2+} release. COP-I subunits play a central role in this mechanism, suggesting that Wnt5a-dependent cell polarity may involve recruitment of the ER via interactions between COP-I and cortical membrane proteins. COP-I is classically associated with Golgi/ERGIC membranes, although there are a few older controversial reports of its presence on the ER or endosomal membranes (Bednarek et al., 1995; Gu and Gruenberg, 2000). In addition, studies in malignant melanoma cells have shown that melanoma inhibitory activity (MIA), an autocrine protein that promotes cancer progression and metastasis, binds integrins $\alpha_4\beta_1$ and $\alpha_5\beta_1$, mediating membrane detachment (Schmidt et al., 2010). MIA is secreted at the trailing edge of cells through processes involving COP-I, as well as localized KCa3.1 K^+ channels, which are activated in response to intracellular Ca^{2+}.

It is very likely that the WRAMP structure underlies processes of cancer cell invasion and metastasis. MCAM is upregulated in metastatic melanoma, and promotes cell invasion from epidermis to dermis in skin reconstruct models (Satyamoorthy et al., 2001). Wnt5a strongly enhances invasion of cultured melanoma cells, and its expression is correlated with advanced stage in melanoma specimens (Weeraratna et al., 2002). How Wnt5a promotes cancer cell invasion by controlling cell polarity is currently unknown. In neuronal cell systems, Wnt5a intersects with atypical PKC and PARtition complex proteins that directly bind Dishevelled and control axon outgrowth through the organization of microtubule and actin dynamics (Zhang et al., 2007; Sun et al., 2001). Our findings show that mechanisms that polarize proteins to the tail end of cells are equally important for Wnt5a-dependent cell movement.

Studies of cancer cell invasion in 3D matrices reveal an important role of rear-end dynamics. Invasion is often classified into separate mechanisms. Mesenchymal mechanisms involve elongated cell morphologies, Rac-dependent leading-edge actin polymerization, integrin β1 polarization, and MMP secretion. Amoeboid mechanisms involve rounded cell morphologies that exclude integrin and MMPs and Rho- and ROCK-dependent tail-end retraction (Sanz-Moreno et al., 2008). In A375 melanoma cells, Lorentzen et al. (2011) described a uropod-like structure, named the "ezrin-radixin-uropod-like structure" (ERULS). The ERULS mediates amoeboid cell invasion by tail-end enrichment of ezrin, phosphorylated ezrin, F-actin, myosin light chain, phosphatidylinositol 4,5-bisphosphate, and integrin β1. The ERULS differs from other uropod structures in its regulation by protein kinase C and membrane attachment at the trailing edge, which in uropods is normally lifted away from the substrate. Like the WRAMP structure, the ERULS is dependent on Rho kinase (Sahai and Marshall, 2003). In WM239A cells, invasion through 3D collagen is clearly mesenchymal (Old et al., 2009), and invasion through 3D hydrogels requires proteolytic degradation and integrin signaling (Figure 1), which differs from the standard view of amoeboid movement. Nevertheless, MCAM binds and recruits ezrin/moesin into cell protrusions in melanoma cells, facilitating cell movement by MCAM binding to RhoGDI1, RhoA activation, and ROCK-dependent ERM phosphorylation (Luo et al., 2012). Thus, it is reasonable to hypothesize that the ERULS represents one form of the WRAMP structure in cells undergoing amoeboid cell movement, although the WRAMP structure appears to be a more general entity observed across different cell types and different invasion mechanisms.

In summary, polarized formation of the WRAMP structure through MCAM-associated MVBs, cytoskeletal membrane attachments, and recruitment of cortical ER provides a working model to explain how Wnt5a promotes invasion by directing the Ca^{2+} mobilization needed for actomyosin contraction and tail-end membrane retraction. Understanding how the composition and regulation of this machinery varies under different cellular contexts will provide new insight into how Wnt5a controls invasion and metastasis through the control of cell polarity.

EXPERIMENTAL PROCEDURES

Materials

Antibodies used were mouse αMCAM, rabbit αEEA1, rabbit αcalnexin, and mouse αDvl2 (Santa Cruz Biotechnology), mouse αIQGAP1 (Invitrogen), mouse αclathrin (BD Transduction), αCOP-Iβ and αGFP (Abcam), and rabbit αmyosin IIb and α58kDa Golgi protein (Sigma). Plasmids expressing MCAM-GFP, IQGAP1-RFP, ER-RFP (from Eric Snapp, Albert Einstein University), myosin II heavy chain-RFP (from Robert Adelstein, NIH), and Cameleon-FRET biosensor (from Roger Tsien, University of California, San Diego) have been described (Witze et al., 2008; Jeong et al., 2007; Snapp et al., 2006; Wei and Adelstein, 2000; Miyawaki et al., 1999). Brefeldin A (Enzo Life Sciences) was added to cells at 10 μg/ml in serum-free RPMI for 2 hr prior to treatment ±Wnt5a.

Cell Culture

WM239A cells were maintained in RPMI+10% FBS. COP-Iβ, IQGAP1, and Dvl2 knockdowns were performed using siGenome SMARTpool or siRNA duplex oligonucleotides (Dharmacon). Cells were preincubated with inhibitors (2.5 μM) or DMSO for 1 hr at 37°C, and media were replaced with RPMI+250-ng/ml Wnt5a. With 2-APB, cells were treated with Wnt5a and monitored live, adding inhibitor at the moment of WRAMP structure formation. For calpain inhibitor III (EMD Millipore), cells were treated with the inhibitor (12 μM in DMSO)+Wnt5a or control buffer simultaneously and imaged live for 1 hr. Immunoprecipitations were performed with αGFP, αDvl2, or αCOP-Iβ antibodies, monitoring pull-downs by western blotting.

Cells were cultured in hydrogels photopolymerized using 4-arm 20,000 MW PEG-norbornene (Fairbanks et al., 2009; Schwartz et al., 2010) crosslinked with peptides KKCG**GPQG↓IWGQ**GCKK, with an MMP-degradable sequence (Nagase and Fields, 1996), and C**RGD**S, with an integrin recognition motif (Ruoslahti and Pierschbacher, 1987). A nonbioactive scrambled peptide, C**RDG**S, was used for control experiments ("0 RGD"). Live images were collected every 0.5 hr for up to 36 hr using a Nikon TE2000E microscope. Immunostaining was performed after 48 hr, collected with a Zeiss LSM5 Pascal scanning confocal microscope. For ROCK inhibition, 10 μM Y27632 (Sigma) was added 2 hr before imaging.

Organelle Proteomics

WM239A (5.3×10^6) cells were treated ±Wnt5a and harvested into lysis buffer (10 mM Tris [pH 8], 1.5 mM $MgCl_2$, 10 mM KCl). Postnuclear supernatants were mixed with iodixanol to a final concentration of 17.5% and overlaid onto 700 μl cushions of 20% iodixanol, and then overlaid with 700 μl 0.25 M sucrose in lysis buffer and centrifuged without braking (350,000 × *g*, 2 hr). Fractions (150 μl) were collected and added to 150 μl lysis buffer followed by centrifugation (60,000 rpm, 20 min). Pellets were washed, resuspended with 0.1% Rapigest, 50 mM NH_4HCO_3, and boiled for 10 min. Proteins were reduced, alkylated, and digested with trypsin (Promega) for 3 hr at 37°C. Rapigest was cleaved with trifluoroacetic acid followed by centrifugation, and the top layer containing the peptides was stored at −80°C.

LC-MS/MS was performed on a Thermo LTQ-Orbitrap mass spectrometer with a Waters nanoAcquity UPLC (BEH-C18 column, 25 cm x 75 μm i.d., 1.7 μm, 100 Å). Peptide digests (2 μg) were separated by a linear gradient

from 95% buffer A (0.1% formic acid) to 40% buffer B (0.1% formic acid, 80% CH_3CN) over 120 min at 300 nl/min. For each MS scan, the ten most intense ions were targeted for MS/MS with dynamic exclusion 30 s, 1 Da exclusion width, excluding ions with charge state +1 or unassigned. The maximum injection time was 500 ms for Orbitrap scans (automatic gain control [AGC] = 1×10^6) and 500 ms for LTQ MS/MS (AGC = 1×10^4).

Microscopy

For immunocytochemistry, 5×10^5 cells were seeded on glass coverslips for 24 hr, washed, and incubated overnight in RPMI. The media were removed, RPMI+150 ng/ml Wnt5a was added, and cells were incubated at 37°C for 30 min. Cells were fixed in 4% formalin at room temperature, permeabilized with 0.1% Triton X-100, blocked with 5% BSA, 0.1% Tween/Tris-buffered saline, and incubated with 1° antibody (1:200 dilution) followed by Alexa Fluor 488 or 594 donkey αmouse or αrabbit 2° antibody (Invitrogen). Images were collected on an Olympus IX81 inverted microscope and analyzed with Slidebook software.

Live-cell imaging was performed in an environmental chamber on an Olympus microscope. Cells were serum starved, washed with Hank's balanced salt solution (HBSS), and incubated in HBSS, 25 mM HEPES (pH 7.4). Images were collected every 30–60 s on GFP and RFP channels with a stage temperature of 35°C. FRET imaging of the Cameleon sensor was performed on a Nikon Eclipse TE2000-S inverted microscope, and images were acquired with a CoolSNAP ES digital camera (Photometrics) and analyzed with MetaMorph software. Calibrations used Ca^{2+}-free conditions (R_{min}) by incubating cells with 5 μM ionomycin, 3 mM EGTA and Ca^{2+}-saturating conditions of 5 μM ionomycin,10 mM $CaCl_2$ (Palmer and Tsien, 2006).

For electron microscopy, cells were prepared as described (McDonald, 1984) with sample fixation in 50 mM sodium cacodylate, 2% glutaraldehyde, and postfixation with 0.5% osmium tetroxide, 0.8% $K_3Fe(CN)_6$. Cells were stained with 0.15% tannic acid, dehydrated in acetone, and embedded in Epon Araldite resin. Images were collected with a Tecnai F-30 electron microscope (FEI) and Gatan CCD camera, recording serial tilts of ±60° in increments of 1° (Mastronarde, 2005). Each section was imaged in two tilt series around orthogonal axes and then assembled into a single reconstruction using IMOD software (Mastronarde, 1997). Tomographic reconstructions were modeled by manual contour tracing using IMOD (Kremer et al., 1996).

SUPPLEMENTAL INFORMATION

Supplemental Information includes Supplemental Experimental Procedures, three figures, two tables, and three movies and can be found with this article online at http://dx.doi.org/10.1016/j.devcel.2013.08.019.

ACKNOWLEDGMENTS

We are indebted to Amy Palmer and William Old for many helpful discussions, Robert Rogers for assistance with 3D cell culture, Kevin Dean for assistance with light microscopy, and Andreas Hoenger for access to the Boulder Laboratory for 3D Electron Microscopy, a National Research Resource. This work was supported by NIH grants F32-CA112847 (E.S.W.), R01-CA118972 (N.G.A.), and P41-RR000592 (to Andreas Hoenger).

Received: August 5, 2011
Revised: June 10, 2013
Accepted: August 28, 2013
Published: September 30, 2013

REFERENCES

Bednarek, S.Y., Ravazzola, M., Hosobuchi, M., Amherdt, M., Perrelet, A., Schekman, R., and Orci, L. (1995). COPI- and COPII-coated vesicles bud directly from the endoplasmic reticulum in yeast. Cell *83*, 1183–1196.

Brandt, D.T., Marion, S., Griffiths, G., Watanabe, T., Kaibuchi, K., and Grosse, R. (2007). Dia1 and IQGAP1 interact in cell migration and phagocytic cup formation. J. Cell Biol. *178*, 193–200.

Brundage, R.A., Fogarty, K.E., Tuft, R.A., and Fay, F.S. (1991). Calcium gradients underlying polarization and chemotaxis of eosinophils. Science *254*, 703–706.

Burridge, K., and Connell, L. (1983). Talin: a cytoskeletal component concentrated in adhesion plaques and other sites of actin-membrane interaction. Cell Motil. *3*, 405–417.

Carragher, N.O., and Frame, M.C. (2004). Focal adhesion and actin dynamics: a place where kinases and proteases meet to promote invasion. Trends Cell Biol. *14*, 241–249.

Colvin, R.A., Means, T.K., Diefenbach, T.J., Moita, L.F., Friday, R.P., Sever, S., Campanella, G.S., Abrazinski, T., Manice, L.A., Moita, C., et al. (2010). Synaptotagmin-mediated vesicle fusion regulates cell migration. Nat. Immunol. *11*, 495–502.

Cramer, L.P. (2010). Forming the cell rear first: breaking cell symmetry to trigger directed cell migration. Nat. Cell Biol. *12*, 628–632.

Eddy, R.J., Pierini, L.M., and Maxfield, F.R. (2002). Microtubule asymmetry during neutrophil polarization and migration. Mol. Biol. Cell *13*, 4470–4483.

Ercan, E., Momburg, F., Engel, U., Temmerman, K., Nickel, W., and Seedorf, M. (2009). A conserved, lipid-mediated sorting mechanism of yeast Ist2 and mammalian STIM proteins to the peripheral ER. Traffic *10*, 1802–1818.

Fairbanks, B., Schwartz, M., Halevi, A., Nuttelman, C., Bowman, C., and Anseth, K. (2009). A versatile synthetic extracellular matrix mimic via thiol-norbornene photopolymerization. Adv. Mater. *21*, 5005–5010.

Fernandez-Borja, M., Janssen, L., Verwoerd, D., Hordijk, P., and Neefjes, J. (2005). RhoB regulates endosome transport by promoting actin assembly on endosomal membranes through Dia1. J. Cell Sci. *118*, 2661–2670.

Gampel, A., Parker, P.J., and Mellor, H. (1999). Regulation of epidermal growth factor receptor traffic by the small GTPase rhoB. Curr. Biol. *9*, 955–958.

Glading, A., Uberall, F., Keyse, S.M., Lauffenburger, D.A., and Wells, A. (2001). Membrane proximal ERK signaling is required for M-calpain activation downstream of epidermal growth factor receptor signaling. J. Biol. Chem. *276*, 23341–23348.

Gu, F., and Gruenberg, J. (2000). ARF1 regulates pH-dependent COP functions in the early endocytic pathway. J. Biol. Chem. *275*, 8154–8160.

Hahn, K., DeBiasio, R., and Taylor, D.L. (1992). Patterns of elevated free calcium and calmodulin activation in living cells. Nature *359*, 736–738.

Jeong, H.W., Li, Z., Brown, M.D., and Sacks, D.B. (2007). IQGAP1 binds Rap1 and modulates its activity. J. Biol. Chem. *282*, 20752–20762.

Kohn, A.D., and Moon, R.T. (2005). Wnt and calcium signaling: β-catenin-independent pathways. Cell Calcium *38*, 439–446.

Kremer, J.R., Mastronarde, D.N., and McIntosh, J.R. (1996). Computer visualization of three-dimensional image data using IMOD. J. Struct. Biol. *116*, 71–76.

Kriebel, P.W., Barr, V.A., Rericha, E.C., Zhang, G., and Parent, C.A. (2008). Collective cell migration requires vesicular trafficking for chemoattractant delivery at the trailing edge. J. Cell Biol. *183*, 949–961.

Lavieu, G., Orci, L., Shi, L., Geiling, M., Ravazzola, M., Wieland, F., Cosson, P., and Rothman, J.E. (2010). Induction of cortical endoplasmic reticulum by dimerization of a coatomer-binding peptide anchored to endoplasmic reticulum membranes. Proc. Natl. Acad. Sci. USA *107*, 6876–6881.

Le Clainche, C., Schlaepfer, D., Ferrari, A., Klingauf, M., Grohmanova, K., Veligodskiy, A., Didry, D., Le, D., Egile, C., Carlier, M.F., and Kroschewski, R. (2007). IQGAP1 stimulates actin assembly through the N-WASP-Arp2/3 pathway. J. Biol. Chem. *282*, 426–435.

Lorentzen, A., Bamber, J., Sadok, A., Elson-Schwab, I., and Marshall, C.J. (2011). An ezrin-rich, rigid uropod-like structure directs movement of amoeboid blebbing cells. J. Cell Sci. *124*, 1256–1267.

Luo, Y., Zheng, C., Zhang, J., Lu, D., Zhuang, J., Xing, S., Feng, J., Yang, D., and Yan, X. (2012). Recognition of CD146 as an ERM-binding protein offers novel mechanisms for melanoma cell migration. Oncogene *31*, 306–321.

Martini, F.J., and Valdeolmillos, M. (2010). Actomyosin contraction at the cell rear drives nuclear translocation in migrating cortical interneurons. J. Neurosci. *30*, 8660–8670.

Mastronarde, D.N. (1997). Dual-axis tomography: an approach with alignment methods that preserve resolution. J. Struct. Biol. *120*, 343–352.

Mastronarde, D.N. (2005). Automated electron microscope tomography using robust prediction of specimen movements. J. Struct. Biol. *152*, 36–51.

McDonald, K. (1984). Osmium ferricyanide fixation improves microfilament preservation and membrane visualization in a variety of animal cell types. J. Ultrastruct. Res. *86*, 107–118.

Miyawaki, A., Griesbeck, O., Heim, R., and Tsien, R.Y. (1999). Dynamic and quantitative Ca^{2+} measurements using improved cameleons. Proc. Natl. Acad. Sci. USA *96*, 2135–2140.

Moser, M., Nieswandt, B., Ussar, S., Pozgajova, M., and Fässler, R. (2008). Kindlin-3 is essential for integrin activation and platelet aggregation. Nat. Med. *14*, 325–330.

Nagase, H., and Fields, G.B. (1996). Human matrix metalloproteinase specificity studies using collagen sequence-based synthetic peptides. Biopolymers *40*, 399–416.

Nakamura, F., Stossel, T.P., and Hartwig, J.H. (2011). The filamins: organizers of cell structure and function. Cell Adhes. Migr. *5*, 160–169.

O'Connell, M.P., Fiori, J.L., Baugher, K.M., Indig, F.E., French, A.D., Camilli, T.C., Frank, B.P., Earley, R., Hoek, K.S., Hasskamp, J.H., et al. (2009). Wnt5A activates the calpain-mediated cleavage of filamin A. J. Invest. Dermatol. *129*, 1782–1789.

Old, W.M., Meyer-Arendt, K., Aveline-Wolf, L., Pierce, K.G., Mendoza, A., Sevinsky, J.R., Resing, K.A., and Ahn, N.G. (2005). Comparison of label-free methods for quantifying human proteins by shotgun proteomics. Mol. Cell. Proteomics *4*, 1487–1502.

Old, W.M., Shabb, J.B., Houel, S., Wang, H., Couts, K.L., Yen, C.Y., Litman, E.S., Croy, C.H., Meyer-Arendt, K., Miranda, J.G., et al. (2009). Functional proteomics identifies targets of phosphorylation by B-Raf signaling in melanoma. Mol. Cell *34*, 115–131.

Orci, L., Ravazzola, M., Le Coadic, M., Shen, W.W., Demaurex, N., and Cosson, P. (2009). STIM1-induced precortical and cortical subdomains of the endoplasmic reticulum. Proc. Natl. Acad. Sci. USA *106*, 19358–19362.

Palmer, A.E., and Tsien, R.Y. (2006). Measuring calcium signaling using genetically targetable fluorescent indicators. Nat. Protoc. *1*, 1057–1065.

Park, C.Y., Hoover, P.J., Mullins, F.M., Bachhawat, P., Covington, E.D., Raunser, S., Walz, T., Garcia, K.C., Dolmetsch, R.E., and Lewis, R.S. (2009). STIM1 clusters and activates CRAC channels via direct binding of a cytosolic domain to Orai1. Cell *136*, 876–890.

Parsons, J.T., Horwitz, A.R., and Schwartz, M.A. (2010). Cell adhesion: integrating cytoskeletal dynamics and cellular tension. Nat. Rev. Mol. Cell Biol. *11*, 633–643.

Petrie, R.J., Doyle, A.D., and Yamada, K.M. (2009). Random versus directionally persistent cell migration. Nat. Rev. Mol. Cell Biol. *10*, 538–549.

Ruoslahti, E., and Pierschbacher, M.D. (1987). New perspectives in cell adhesion: RGD and integrins. Science *238*, 491–497.

Sahai, E., and Marshall, C.J. (2003). Differing modes of tumour cell invasion have distinct requirements for Rho/ROCK signalling and extracellular proteolysis. Nat. Cell Biol. *5*, 711–719.

Salas-Cortes, L., Ye, F., Tenza, D., Wilhelm, C., Theos, A., Louvard, D., Raposo, G., and Coudrier, E. (2005). Myosin Ib modulates the morphology and the protein transport within multi-vesicular sorting endosomes. J. Cell Sci. *118*, 4823–4832.

Sánchez-Madrid, F., and Serrador, J.M. (2009). Bringing up the rear: defining the roles of the uropod. Nat. Rev. Mol. Cell Biol. *10*, 353–359.

Sanz-Moreno, V., Gadea, G., Ahn, J., Paterson, H., Marra, P., Pinner, S., Sahai, E., and Marshall, C.J. (2008). Rac activation and inactivation control plasticity of tumor cell movement. Cell *135*, 510–523.

Satyamoorthy, K., Muyrers, J., Meier, F., Patel, D., and Herlyn, M. (2001). Mel-CAM-specific genetic suppressor elements inhibit melanoma growth and invasion through loss of gap junctional communication. Oncogene *20*, 4676–4684.

Schmidt, J., Friebel, K., Schönherr, R., Coppolino, M.G., and Bosserhoff, A.K. (2010). Migration-associated secretion of melanoma inhibitory activity at the cell rear is supported by KCa3.1 potassium channels. Cell Res. *20*, 1224–1238.

Schwartz, M.P., Fairbanks, B.D., Rogers, R.E., Rangarajan, R., Zaman, M.H., and Anseth, K.S. (2010). A synthetic strategy for mimicking the extracellular matrix provides new insight about tumor cell migration. Integr. Biol. (Camb.) *2*, 32–40.

Snapp, E.L., Sharma, A., Lippincott-Schwartz, J., and Hegde, R.S. (2006). Monitoring chaperone engagement of substrates in the endoplasmic reticulum of live cells. Proc. Natl. Acad. Sci. USA *103*, 6536–6541.

Sun, T.Q., Lu, B., Feng, J.J., Reinhard, C., Jan, Y.N., Fantl, W.J., and Williams, L.T. (2001). PAR-1 is a Dishevelled-associated kinase and a positive regulator of Wnt signalling. Nat. Cell Biol. *3*, 628–636.

Wallar, B.J., Deward, A.D., Resau, J.H., and Alberts, A.S. (2007). RhoB and the mammalian Diaphanous-related formin mDia2 in endosome trafficking. Exp. Cell Res. *313*, 560–571.

Wang, Q., Herrera Abreu, M.T., Siminovitch, K., Downey, G.P., and McCulloch, C.A. (2006). Phosphorylation of SHP-2 regulates interactions between the endoplasmic reticulum and focal adhesions to restrict interleukin-1-induced Ca^{2+} signaling. J. Biol. Chem. *281*, 31093–31105.

Weeraratna, A.T., Jiang, Y., Hostetter, G., Rosenblatt, K., Duray, P., Bittner, M., and Trent, J.M. (2002). Wnt5a signaling directly affects cell motility and invasion of metastatic melanoma. Cancer Cell *1*, 279–288.

Wei, Q., and Adelstein, R.S. (2000). Conditional expression of a truncated fragment of nonmuscle myosin II-A alters cell shape but not cytokinesis in HeLa cells. Mol. Biol. Cell *11*, 3617–3627.

Wei, C., Wang, X., Chen, M., Ouyang, K., Song, L.S., and Cheng, H. (2009). Calcium flickers steer cell migration. Nature *457*, 901–905.

Witze, E.S., Litman, E.S., Argast, G.M., Moon, R.T., and Ahn, N.G. (2008). Wnt5a control of cell polarity and directional movement by polarized redistribution of adhesion receptors. Science *320*, 365–369.

Wu, M.M., Buchanan, J., Luik, R.M., and Lewis, R.S. (2006). Ca^{2+} store depletion causes STIM1 to accumulate in ER regions closely associated with the plasma membrane. J. Cell Biol. *174*, 803–813.

Yamada, M., Toba, S., Takitoh, T., Yoshida, Y., Mori, D., Nakamura, T., Iwane, A.H., Yanagida, T., Imai, H., Yu-Lee, L.Y., et al. (2010). mNUDC is required for plus-end-directed transport of cytoplasmic dynein and dynactins by kinesin-1. EMBO J. *29*, 517–531.

Yin, H.L., and Stossel, T.P. (1979). Control of cytoplasmic actin gel-sol transformation by gelsolin, a calcium-dependent regulatory protein. Nature *281*, 583–586.

Zhang, X., Zhu, J., Yang, G.Y., Wang, Q.J., Qian, L., Chen, Y.M., Chen, F., Tao, Y., Hu, H.S., Wang, T., and Luo, Z.G. (2007). Dishevelled promotes axon differentiation by regulating atypical protein kinase C. Nat. Cell Biol. *9*, 743–754.